Photodissociation of ICN at the Water/Chloroform Interface†

Mindy L. Johnson and Ilan Benjamin*

Department of Chemistry and Biochemistry, University of California, Santa Cruz, California 95064

Received: January 7, 2009; Revised Manuscript Received: February 18, 2009

The photodissociation of ICN adsorbed at the water/chloroform liquid−liquid interface is studied using semiclassical molecular dynamics with nonadiabatic surface hopping. Several fundamental processes following the bond breakup of ICN adsorbed at the interface are compared with the same processes taking place in bulk water and bulk chloroform. These include cage escape, rotational relaxation of the CN product, recombination on the ground state to form ICN and INC, and their vibrational relaxation. The probability for cage escape at the liquid/liquid interface is larger than in the bulk of either liquid. Nonadiabatic transitions among the different electronic states have rates that are very similar in bulk water and at the interface but slightly more rapid in chloroform. The translational and rotational relaxation of the photofragments strongly depend on the final photodissociation outcome, but typically the dynamics in bulk water are slightly faster than at the water/chloroform interface and typically much faster than the behavior in bulk chloroform. The vibrational excitation of the ICN and INC products relaxes much slower in bulk chloroform than in bulk water, with the interface results falling in between, closer to the bulk water dynamics.

I. Introduction

Photodissociation reactions in heterogeneous environments are of great interest to many areas of science and technology. Many decades of work have provided much understanding of these reactions at solid surfaces, in micelles, in proteins, and in other biological systems. These studies, together with the much older (but still active) studies of photodissociation in bulk liquids and in clusters, provide a comprehensive yet still evolving understanding of the effect of the condensed phase on cage escape, geminate recombination, and product energy distribution.

One area of heterogeneous photochemistry that is beginning to attract growing attention is that of photodissociation of adsorbed molecules at liquid interfaces. Several experimental and theoretical studies on photodissociation at the gas−liquid interface have appeared. Some of these experimental studies, which are of great importance to atmospheric chemistry, include photodissociation of alkyl iodide, alkyl nitrite, and 4-iodobenzoic acid adsorbed at the liquid/vapor interface of glycerol and squalane studied by time-of-flight quadrupole mass spectroscopy[1,2] and photodissociation of OClO, Cl_2, and $CFCl_3$ adsorbed on water ice surfaces.[3,4] We used molecular dynamics simulations to examine the photodissociation dynamics of ICN adsorbed at the surface of liquid chloroform[5] and water[6] and the photodissociation of OClO adsorbed at the surface of water, ethanol, and acetonitrile.[7] Some of the main results of these studies include the following. (1) The probability for photoproduct cage escape is significantly enhanced when the reaction takes place at the liquid/vapor interface due to the more "fluid" nature of the solvent cage. (2) The probability for cage escape and the desorption of the photoproducts depends on the initial location and orientation of the parent molecule. (3) Vibrational relaxation of the recombined parent molecule is slower than in the bulk by a factor of 3−4.

One area of photoreaction dynamics that has not been studied computationally is that of photodissociation reactions at liquid/liquid interfaces. These reactions are clearly important for the design of energy conversion and storage devices, as well as in the development of photosurfactants. Photoreactions at liquid/liquid interfaces have been studied experimentally using nonlinear optical methods,[8−11] and clearly the much investigated photoreactions in micelles, including photodissociation reactions,[12,13] are closely related to the photochemistry at liquid/liquid interfaces.

In this paper, we extend our previous studies on the photodissociation of ICN to examining this reaction at the water/chloroform interface. The choice of this particular system is motivated by the fact that this reaction has been studied experimentally and theoretically in the bulk of each of these liquids. In addition, the water/chloroform interface is of much interest in many areas of analytical and surface chemistry, and its neat structure has been the focus of several experimental and theoretical studies.[14−16]

Our focus is on the following questions: What is the influence of the water/chloroform surface region on the different aspects of the photodissociation dynamics mentioned above, and how are the dynamics compared with the dynamics in each of the two bulk liquids? Unlike at the liquid/vapor interface, the liquid/liquid interface does not have a reduced density region that may enhance cage escape. On the other hand, there is a significant change in the polarity of the media across the interface that may affect the reaction. Also, trapping and geminate recombination may be influenced by the possibility that the solvent cage is made of both water and chloroform molecules, whose mutual interaction is weaker than the molecules in bulk water.

The rest of the paper is organized as follows: In section II, we describe the potential-energy functions of the solute and solvent molecules. In section III, we describe the method used to compute the spectra and the photodissociation dynamics. In section IV, we discuss the results, including product state distribution, caging effects, and recombination to produce ICN and INC. We conclude in section V with a summary.

† Part of the "Robert Benny Gerber Festschrift".

* To whom correspondence should be addressed.

10.1021/jp900153j CCC: $40.75 © 2009 American Chemical Society
Published on Web 03/26/2009

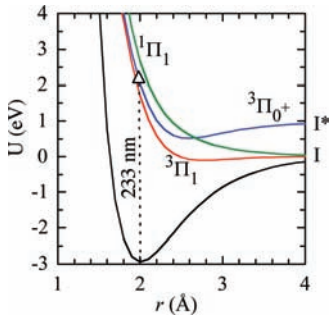

Figure 1. Ground-state and three excited states comprising the A band of ICN as a function of the I−C bond distance for CN at its equilibrium geometry (in ICN) and a linear geometry, calculated using the functional form given in ref 19.

II. Potential-Energy Functions

1. ICN Ground and Excited Potential-Energy Surfaces. The ICN UV A band is comprised of three different electronic states ($^3\Pi_1$, $^3\Pi_{0+}$, and $^1\Pi_1$) that are accessible by excitation of the ground-state ICN ($^1\Sigma^+$). There are two photodissociation channels producing CN in its ground electronic state and either ground-state iodine I($^2P_{3/2}$) or an excited-state iodine I* ($^2P_{1/2}$) atom. The energy difference between these two channels corresponds to the spin−orbit splitting of iodine (21.7 kcal/mol). As in our previous studies,[5,6,17] we use the ab initio surfaces computed by Morokuma and co-workers.[18,19] These surfaces have been used by several groups to study different aspects of ICN photodissociation in the gas phase[20] and in solid Ar,[21,22] with reasonable agreement with experiments. Figure 1 shows the three excited states and the ground state as a function of the I−C bond distance for the linear ICN geometry. A complete description of these surfaces, including the analytical fits used in the molecular dynamics simulation, can be found in the above references. Here we briefly review some important features of these surfaces.

For reasons discussed below, we study the photodissociation of ICN following excitation with a 233 nm UV light. At this energy, only the two triplet excited states, $^3\Pi_1$ and $^3\Pi_{0+}$, are accessible. The $^3\Pi_{0+}$ excited state is bent in the Franck−Condon region, so that the CN fragment is produced initially rotationally hot. This state correlates with the I* + CN fragments, and so it is at least 1 eV higher in energy than the I + CN asymptotic region. The $^3\Pi_{0+}$ and $^1\Pi_1$ excited states have a single crossing in the region 2.6 Å < r_{IC} < 3.0 Å at each value of the ICN bending angle θ, and they are strongly coupled in the crossing region. An analytical expression for this coupling as a function of the ICN geometry has been calculated by Morokuma and co-workers.[19] The $^1\Pi_1$ state crosses the ground state at one or two values of r_{IC}, depending on the bending angle. The $^3\Pi_1$ state asymptotically approaches the ground state at large values of r_{IC} but never crosses it for any value of θ. The coupling between the excited states and the ground state at large distances can be approximately evaluated using the diatomic-in-molecules (DIM) treatment.[23,24] We use a simpler approach, which will be discussed in the methodology section below. Depending on the ICN bending angle, the recombination of the I and CN fragments may produce either ground-state ICN or the isomer INC.

2. Water and Chloroform Potentials. The water−water, chloroform−chloroform, and water−chloroform potentials are described using a pairwise sum of Lennard−Jones + Coulomb terms

$$u_{ij} = 4\varepsilon_{ij}\left[\left(\frac{\sigma_{ij}}{r_{ij}}\right)^{12} - \left(\frac{\sigma_{ij}}{r_{ij}}\right)^{6}\right] + \frac{q_i q_j}{4\pi\varepsilon_0 r_{ij}} \quad (1)$$

where i and j are two atomic sites in two different molecules, r_{ij} is the distance between the sites, and ε_0 is the universal constant (vacuum permittivity). The Lennard−Jones parameters between different sites are determined using the atomic parameters listed in Table 1 and the usual mixing rules

$$\sigma_{ij} = (\sigma_{ii} + \sigma_{jj})/2, \varepsilon_{ij} = \sqrt{\varepsilon_{ii}\varepsilon_{jj}} \quad (2)$$

The water potential is a flexible simple point charge[25] (SPC) model we have used extensively in the past and has been shown to give a reasonable description of bulk and interfacial water.[26] The water intramolecular potential-energy function is the spectroscopic potential of Kuchitsu and Morino.[27] The chloroform intramolecular potential is based on a harmonic force field, with bond stretching and bending constants given elsewhere.[28] This potential gives a reasonable description of the properties of bulk and surface chloroform.[28]

3. Interaction Potentials ICN−Water and ICN−Chloroform. The interaction potentials between the ground and excited states of ICN and the water and chloroform molecules is also modeled using Lennard−Jones plus Coulomb terms between each of the ICN atoms and each site on the water and the chloroform molecules. The Lennard−Jones (LJ) parameters are determined using the combination rule for mixtures and the atomic site parameters for the ICN molecule given in Table 1. We use the same LJ parameters for the ground and excited states of ICN.

The charges on the ICN atoms depend on the geometry and electronic state of the molecule. While a full quantum description of these excited states in water involving the CN radical and the two spin states of iodine is desirable, we use a simple empirical approach, which can be incorporated into the classical molecular dynamics simulation. We use a simple switching function, which makes each of the charges on the I, C, and N atoms dependent on the geometry and the electronic state of ICN. A combination of ab initio calculations, electronic absorption spectra calculations, and experimental dipole moment values is used to parametrize this switching function, whose functional form is given elsewhere.[17]

Note that while all the intermolecular potential-energy functions used are pairwise additive, the polarizable nature of the solvent and solute molecules is effectively included by proper adjustment of the Lennard−Jones parameters and the point charges. Using many-body polarizable potentials,[29−43] which were found to be more accurate for ions at interfaces, is not expected here to make a fundamental difference, but this should be explored in future studies.

III. Methodology

In this section, we describe the procedure we use to generate an ensemble of photodissociation trajectories. This includes the following steps. (1) Equilibrating a single ICN molecule at the water/chloroform interface. (2) Calculating the absorption spectrum from an equilibrium trajectory on the ground state of ICN. (3) Generating the initial conditions for the photodissociation calculations. (4) Using the initial conditions to run the dissociation trajectories with a surface-hopping algorithm. All the molecular dynamics calculations are done using a time step of 0.5 fs and the velocity version of the Verlet algorithm. Steps

TABLE 1: Lennard−Jones and Coulomb Parameters

atom	σ (Å)	ε (kcal/mol)	q (au)
H(H_2O)	0	0	0.41
O	3.16554	0.1554	−0.82
C($CHCl_3$)	3.2	0.101	0.32
H($CHCl_3$)	2.75	0.0266	0.10
Cl	3.5	0.348	−0.14
I	3.81	0.476	see ref 17
C (ICN)	3.35	0.101	
N	3.31	0.074	

1−3 are done at a fixed temperature of 293 K. The trajectories in step 4 are run at constant energy.

1. System Preparation and Equilibration. The system includes a single ICN molecule, 500 water molecules, and 213 chloroform molecules in a rectangular box of dimensions 24.83 Å × 24.83 × 100 Å, such that the liquid/liquid interface is perpendicular to the long Z axis of the simulation box. In order to increase the sampling statistics, during the equilibrium simulation used to compute the spectra and the initial conditions for the photodissociation calculations, the ICN molecule is constrained to be in a 3 Å wide window centered at the Gibbs dividing surface (which is taken to be at $Z = 0$ and is approximately the plane where the water density is 50% of the bulk value). This constraining potential is removed during the photodissociation calculations. Periodic boundary conditions are used in all three dimensions, with a molecule-based force-switching function. The interface calculations are compared with calculations carried out separately in bulk water using 1000 water molecules in a truncated octahedron box enclosed in a cube of size 39.11 Å and in bulk chloroform using 215 chloroform molecules in a truncated octahedron box enclosed in a cube of size 38.68 Å.

The probability distribution of the equilibrium ICN center of mass position along the Z dimension superimposed on the density profiles of water and chloroform is depicted in Figure 2. The probability distribution peaks at the location of the Gibbs surface, suggesting a local free energy minimum, despite the polar nature of ICN. An examination of the different contributions to the solvation energy at the interface shows that there is a significant contribution from favorable ICN−chloroform interactions due to the effective polarizability of the solvent molecules, as well as significant electrostatic interactions with interfacial water molecules. Specifically, the water−ICN interaction energy at the interface is −17.8 ± 0.2 kcal/mol, 88% of it is electrostatic, compared with the $CHCl_3$−ICN interaction of −5.5 ± 0.1 kcal/mol, only 24% of which is electrostatic. In contrast, the interaction energy of ICN in bulk water is −22.8 ± 0.2 kcal/mol and of ICN in bulk chloroform −16.6 ± 0.2 kcal/mol.

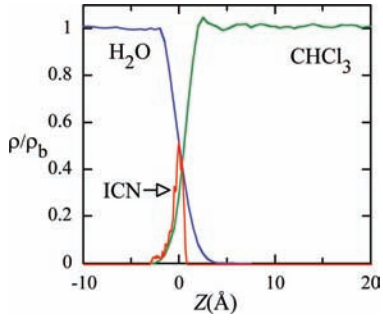

Figure 2. Density profiles (normalized by the bulk densities) of water (blue line) and chloroform (green line) and the probability distribution (arbitrary units, red line) of the center of mass of ICN along the interface normal, calculated from a 1 ns trajectory at 293 K.

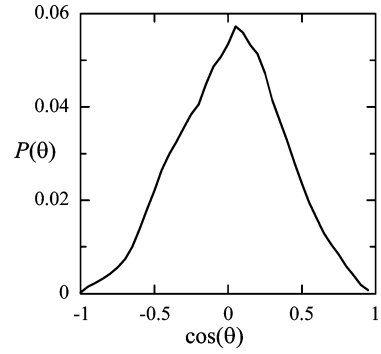

Figure 3. Probability distribution of the angle θ between ICN and the normal to the water/chloroform interface, calculated from a 1 ns trajectory at 293 K.

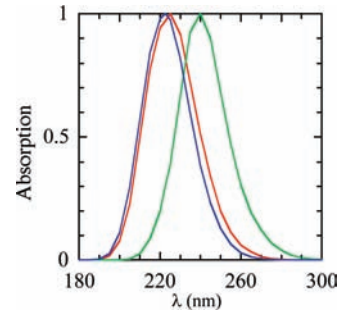

Figure 4. Calculated UV absorption spectrum for the X → $^3\Pi_{0+}$ transition of ICN at 293 K in bulk water (blue) and bulk chloroform (green) and at the water/chloroform interface (red).

The ICN molecule prefers to lie approximately flat with respect to the Gibbs surface, as shown by the orientational distributions given in Figure 3. The distribution of the Z positions and orientations of the ICN molecule in the Franck−Condon configurations (not shown) are approximately the same as the equilibrium distributions.

2. Electronic Absorption Spectra Calculations. A 400 ps trajectory at $T = 293$K is used to compute the electronic absorption spectrum for each of the ICN excited states using the classical Franck−Condon approximation

$$I_\nu(\omega) = \omega(1 - e^{-\hbar\omega/kT})\langle|\mu_\nu(\mathbf{r})|^2\delta[\omega - \Omega_\nu(\mathbf{r})]\rangle_g \quad (3)$$

where $\mu_\nu(\mathbf{r})$ is the electronic transition dipole moment as a function of the nuclear positions $\mathbf{r}$ for the ground to the ν excited state. The ensemble average in eq 3 is over the ground state, and $\hbar\Omega_\nu(\mathbf{r}) = V_\nu(\mathbf{r}) - V_{gr}(\mathbf{r})$ is the energy gap between the ground state and one of the excited states for a particular nuclear configuration. We take the electronic transition dipole moment $\mu_\nu(\mathbf{r})$ to be a constant, and we use the gas-phase oscillator strengths for the excitation to the three different potential energy surfaces to determine the absorption cross section for the individual transitions.

In Figure 4, we compare the calculated absorption spectra for ICN at the liquid/liquid interface with the calculated spectrum in bulk water and bulk chloroform. We show only the spectrum for the transition that carries the largest oscillator strength X → $^3\Pi_{0+}$, which determines the center of the band. The calculated bulk spectra are in good agreement with the experimental results, which peak at 222 nm in water and 240 nm in chloroform. The spectrum at the liquid/liquid interface is very close to that in bulk water, reflecting the tendency of the polar ICN ground state to favorably interact with interfacial

water molecules. The spectral lines corresponding to the other transitions behave in a similar way. All the spectra are blue shifted relative to the gas phase (which peaks at 250 nm) because of the polar solvation of the ground state. The slight increase in the width of the spectra at the interface relative to the bulk is consistent with the higher degree of inhomogeneity at the interface.

3. Initial Conditions for the Photodissociation Trajectories. The classical Franck−Condon (FC) initial conditions for the photodissociation dynamics are found using an iterative procedure, which involves forward and backward integration of the classical equation of motion on the ground electronic state with a variable integration time step in order to find configurations for which $\hbar\omega = V_v(\mathbf{r}) - V_{gr}(\mathbf{r})$ for the given photon energy. (For other methods, see ref 44 and references therein.) Our choice of the photon wavelength of 233 nm is motivated by the fact that this approximately corresponds to the midpoint of the maximum spectrum in the bulk of the two solvents and by the availability of experimental data in bulk water with this wavelength. With this photon energy, either of the two $^3\Pi_{0+}$ and $^3\Pi_1$ excited states are accessible. We use this procedure to select 100 independent FC conditions for each of the two states. This is done for ICN at the liquid/liquid interface as well as in the bulk of each solvent.

4. Nonadiabatic Photodissociation Dynamics. Each of the 100 independent Franck−Condon configurations is used with 10 different initial velocities (selected randomly from a Boltzmann distribution at 293 K) for a total of 1000 trajectories starting on each of the two excited states. Each of the 6000 trajectories (at the interface and in the bulk of the two solvents) is followed for 10 ps, which is typically long enough to decide the outcome of the trajectory, as will be seen below. While one may use the experimentally known oscillator strength to weigh the contribution of each of the two excited states to the overall dynamics, we report the results starting on the two excited states separately.

Due to the coupling between the $^3\Pi_{0+}$ and $^1\Pi_1$ excited states and between the ground state (notation, $^1\Sigma^+$ or X) and the $^3\Pi_0$ and $^1\Pi_1$ states, nonadiabatic transitions between these states must be included for a proper description of the dynamics. There are several methods for treating quantum transitions in a small molecular system interacting with a much larger classical bath.[45] We choose to use the surface-hopping algorithm developed by Tully,[46] which we used to study the 266 nm photodissociation of ICN in water.[6,17] A similar method has been used to study the ICN photodissociation in cryogenic matrices.[21,22] The method involves self-consistent solution of the time-dependent Schrödinger equation for the wave function and of the classical equations for the nuclear degrees of freedom. At each time step, a decision is made whether to switch to a different electronic state using a set of "jump" probabilities. These probabilities are determined by solving the time-dependent quantum equations of motion. Once a decision is made, the atoms are propagated classically on the new surface (or the old surface if no switch was made). The classical propagation on the surface changes the parameters in the quantum Hamiltonian, so the solution of the quantum equations of motion for the new time step provides the next set of transition probabilities.

Briefly, the electronic wave function for ICN is written as

$$|\Psi\rangle = \sum_j^4 c_j(t)|\varphi_j\rangle \tag{4}$$

where the $\{\phi_j\}$ are the four diabatic electronic states ($^1\Sigma^+$, $^3\Pi_1$, $^3\Pi_{0+}$, and $^1\Pi_1$) of ICN. Substitution in the time-dependent Schrödinger equation gives the following four coupled differential equations for $c_j(t)$

$$\frac{\partial c_j}{\partial t} = \frac{i}{\hbar}\sum_k V_{jk}[\mathbf{R}(t)]c_k(t) \tag{5}$$

where V_{kk}, $k = 1-4$, are the diabatic potential-energy surfaces of Amatatsu et al.[19] and V_{jk} is the coupling between states j and k, all calculated using the instantaneous positions $\mathbf{R}(t)$ of the ICN atoms. The coupled differential equations in eq 5 are solved using a fourth-order Runge−Kutta algorithm[47] with an integration time step Δt. The transition probability from state j to state k is then given by[21,22,46]

$$p_{jk} = \frac{\Delta t}{\hbar}\frac{2\mathrm{Im}\{c_j(t)V_{jk}c_k^*(t)\}}{|c_j(t)|^2} \tag{6}$$

The transition probabilities from state j to all other states are used to determine to which state (if any) the system will jump. Energy and momentum conservation is maintained by adjusting the velocities of the ICN atoms. Transitions where p_{jk} is negative or the final kinetic energy is less than zero are rejected. As discussed by Tully,[46] the above algorithm is valid if $|c_j(t)|^2 \approx |c_j(t+\Delta t)|^2$, which in the present simulation requires $\Delta t \approx 0.005$ fs. To avoid using such a short time step for the integration of the nuclear degrees of freedom, we employ a variable integration time step.

The above procedure involves several approximations in addition to those involved in the use of the surface-hopping method.[45] First, we neglect the effect of the solvents on the off-diagonal coupling between the excited states. This may be a reasonable approximation in the initial pass through the crossing region, since the solvent is essentially frozen on this time scale (which happens less than 50 fs after excitation and accounts for most of the surface hopping, as will be described below). Second, while some influence of the solvent on the diagonal (diabatic) curves is included through the charge switching function, this function is parametrized to be a function of solute geometry only. A generalized empirical valence bond (EVB) type approach may be a better representation of the "feedback" effect provided by the solvent,[48−51] but this requires extensive ab initio calculation of excited states of ICN in water clusters. Finally, the gas-phase potentials of Morokuma do not include coupling to the ground state. We assume an irreversible jump from any excited state to the ground state whenever the energy difference between the states (including solvent interaction) is equal or less than kT. While it is possible to use the DIM[23,24] method to obtain a coupling term (in simple cases of weakly interacting solvent and solute), this method may not be reliable in our case. We expect our approximation to somewhat overestimate the actual rate for transitions to the ground state.

It is highly desirable to test the validity of the above approximations with the help of a more fully quantum approach to this reaction (perhaps with ab initio molecular dynamics of the solute in a small cluster of water molecules). However, the exact way that the quantum effects are treated in the present work may not be crucial for our goal of understanding liquid surface effects on the reaction dynamics.

IV. Results and Discussion

The 233 nm photon carries an energy of 55 kcal/mol above the energy of the separate I and CN fragments in the gas phase.

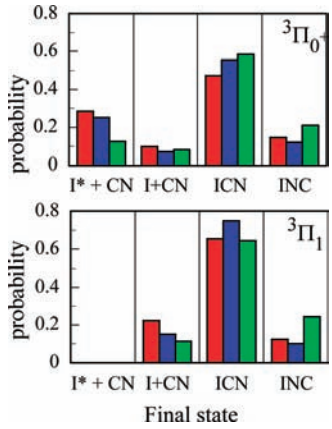

Figure 5. Probability of observing different final products following photodissociation of ICN on the $^3\Pi_{0+}$ (top) and $^3\Pi_1$ (bottom) excited states. In each panel, the blue, green, and red histograms correspond to the reaction in bulk water and bulk chloroform and the water/chloroform interface.

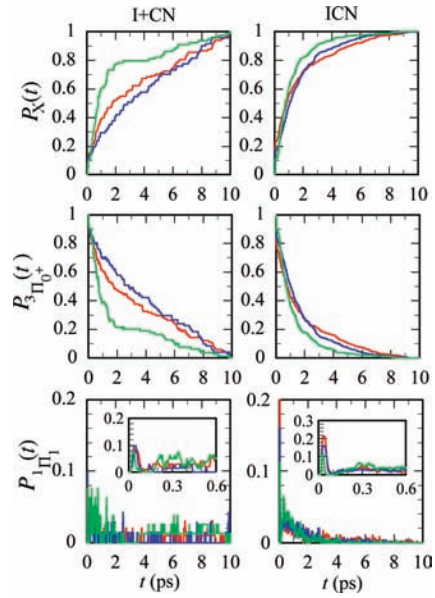

Figure 6. Normalized, time-dependent population of the ground state (X) and the $^3\Pi_{0+}$ and $^1\Pi_1$ excited states following photodissociation of ICN on the $^3\Pi_{0+}$ state that end up as I + CN (left) or ICN (right). Blue, green, and red lines are for the reaction in bulk water and bulk chloroform and at the water/chloroform interface.

Due to the solvation of the polar ground-state ICN relative to these fragments, the average energy available to the fragments in bulk chloroform is about 50 and 40 kcal/mol in bulk water. The spectrum discussed above suggests that the energy available to the fragments at the interface is also close to 40 kcal/mol. The energy available to the I* + CN fragments is reduced by the value of the I/I* splitting (21.7 kcal/mol). We report below the results of the photodissociation calculations, starting with the two different electronic states that are directly accessible with the 233 nm photon. (1) Photodissociation on the $^3\Pi_1$ state produces ground-state iodine. This may follow with recombination on the ground state to form ICN or INC. (2) Photodissociation on the $^3\Pi_{0+}$ state produces excited-state iodine. However, crossing to the $^1\Pi_1$ state, which correlates with I + CN, may lead to transitions to the ground state and recombination.

Our focus in the discussion below is on the way in which the surface region affects different aspects of the dynamics compared with the dynamics in the two bulk liquids. This includes the nonadiabatic transitions, cage escape, recombination, isomerization to produce INC, and, finally, the vibrational relaxation. We define cage escape by the requirement that the distance between the I or the I* and the CN is larger than 6 Å. At this configuration, a water molecule can prevent these two species from recombining. Clearly, due to diffusion, the separated I (or the I*) and CN fragments may recombine later, but this is considered here nongeminate recombination, and it is independent of the photodissociation process. In chloroform, the CN radical may undergo a hydrogen abstraction reaction, but this takes place on the hundreds of picoseconds time scale.

Figure 5 summarizes the probability for the photodissociation fragments to cage escape (as I + CN or I* + CN) or recombine to produce ICN or the isomer INC in the three different media for dissociation, starting from the $^3\Pi_{0+}$ (top) and the $^3\Pi_1$ (bottom) states. We find that while the probability for cage escape at the liquid/liquid interface is larger than in the bulk of either liquid, it is still quite low compared to that at the liquid/vapor interface of either liquid.[5,6] While a precise comparison with experiments is difficult due to the fact that our model is not capable of determining the correct weighting to attach to the ensemble of the trajectories run on the $^3\Pi_{0+}$ and $^3\Pi_1$ states, qualitatively our results in the bulk of the two liquids compare favorably with experimental estimates. [52−55] In bulk water, depending on the relative weight given to the trajectories on these two states, the probability for cage escape is between 15% and 32%, while in bulk chloroform it is between 11% and 21%. In contrast, at the water/chloroform interface it is between 22% and 38%.

1. Nonadiabatic Transitions. We first consider the time scale and probability of the possible nonadiabatic surface hopping. This includes the $^3\Pi_{0+} \rightarrow {}^1\Pi_1$ transitions for the trajectories that started on the $^3\Pi_{0+}$ state and the transitions to the ground state (labeled X) from the $^1\Pi_1$ and $^3\Pi_1$ states.

The transitions $^3\Pi_{0+} \rightarrow {}^1\Pi_1$ may occur very early (<50 fs) on the first pass through the crossing region or later when the I* and CN linger near the crossing region after a collision with the solvent cage removes most of their relative translational energy. Figures 6 and 7 show the population of the various states following photodissociation on the $^3\Pi_{0+}$ state and on the $^3\Pi_1$ state, respectively. The time-dependent populations are shown separately for the trajectories that end up as I + CN or ICN and are normalized by the population of the final outcome. The results when the final product is INC are very similar to the case of ICN and are not shown. The results when the final products are I* + CN do not require a plot, but they are discussed first.

In water, all the trajectories that ended up as I* + CN (in the $^3\Pi_{0+}$ state) went through the crossing region without multiple transitions with the $^1\Pi_1$ state. In chloroform and at the interface, a small percentage (5% and 2%, respectively) experienced some multiple transitions with the $^1\Pi_1$ state. This is due to the fact that the larger energy available to the I* + CN fragments in chloroform, compared with water, increases the chance that if these fragments did not escape the cage, the hard collision with a solvent molecule (at approximately $t = 100$ fs) makes them recoil back to the crossing region (at approximately $t = 200$ fs and again at approximately $t = 400$ fs).

In contrast with the case where the final outcome is I* + CN, the bottom panels of Figure 6 show that transitions to the $^1\Pi_1$ state continue throughout the 10 ps trajectories that lead to ground-state products. (By $t = 10$ ps, all trajectories have either transferred to the ground state or end up as I* + CN.) The nonadiabatic transitions that lead to the I + CN products occur

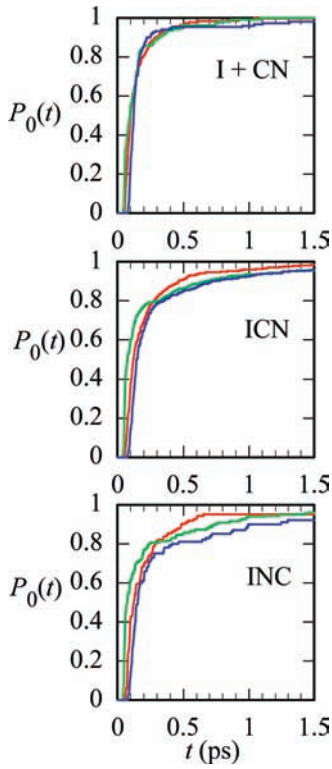

Figure 7. Normalized time-dependent population of the ground state following photodissociation of ICN on the $^3\Pi_1$ excited state leading to I + CN, ICN, or INC (from top to bottom). Blue, green, and red lines are for the reaction in bulk water and bulk chloroform and at the water/chloroform interface.

almost evenly during the trajectory but with a more rapid rate in chloroform than in water or at the interface. As a result, the buildup of the ground-state population is faster in chloroform than in water or at the interface (top panels). The trajectories that lead to ICN experience most of the nonadiabatic transitions early in the trajectories, and the increase in ground-state populations is faster than the increase that leads to I + CN and similar in all three media. It is interesting to note that the first pass through the crossing region has about 50% fewer $^3\Pi_{0+} \rightarrow {}^1\Pi_1$ transitions in chloroform than in water or at the interface, due to the fact that in chloroform the crossing of the region where these two electronic states are coupled is done with a higher speed, and a simple Landau−Zener surface-hopping model would predict smaller jump probabilities.[56] However, later the rate of these transitions in chloroform exceeds the rate in water and at the interface. As a result, the I*/I ratio in chloroform is smaller than in water and at the interface.

The trajectories run on the $^3\Pi_1$ excited state have very different dynamics. The only transitions to consider are to the ground state. Figure 7 shows the populations of the ground-state ICN for the trajectories that end up as I + CN, ICN, and INC, separately. They are normalized by the final value of the population in each channel. In all systems, after a time delay (that ranges from about 40 fs in chloroform to 80 fs in water, corresponding to the time it takes for the fragments to fall off most of the repulsive part of the potential), a rapid increase in the population follows a much slower transfer of the remaining small part of the population to the ground state. Except for the variable delay mentioned above, no significant difference in the rate of the transitions is observed in the different media.

2. Cage Escape vs Recombination. The discussion above about the quantum state dynamics allows us to elucidate the rate of cage escape vs recombination of the I and CN products.

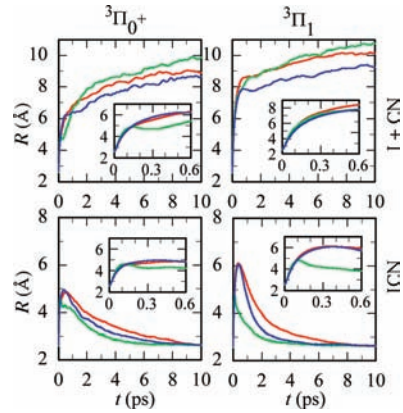

Figure 8. Time-dependent ensemble average of the distance between I and the center of mass of CN following photodissociation of ICN on the $^3\Pi_{0+}$ (left) and $^3\Pi_1$ (right) excited states. The top panels correspond to all the trajectories that ended up as separate I and CN fragments and the bottom panels to the trajectories in which the final product is ICN. In each panel, the blue, green, and red lines correspond to the reaction in bulk water and bulk chloroform and at the water/chloroform interface. The insert in each panel shows the subpicosecond behavior.

The average time scale for recombination and cage escape can be inferred from the average time-dependent distance between the iodine atoms and the center of mass of the CN fragment. This is shown in Figure 8 for the trajectories that recombined as ICN and for the trajectories that ended up as I + CN in the three different media.

The very rapid increase during the first 80 fs corresponds to the descent of the ICN along the exponentially repulsive potential-energy surface. During this time period, the solvent molecules have not yet had time to modify the solute dynamics, and thus, this part of the trajectories is identical for all systems and for all the channels (including the trajectories that resulted in the production of INC and I* + CN, which we do not show). Past this time point and for the next 0.5 ps, the results of all the systems are still nearly identical, except for the trajectories that recombined in bulk chloroform (see the insert), which show the fragments already moving toward each other. Beginning at $t = 0.6$ ps, the trajectories that recombined show a very rapid back collision of the I and CN on the $^3\Pi_1$ state and a more gradual movement for the trajectories that started on the $^3\Pi_{0+}$ state. This is due to the fact that these trajectories spend more time on the excited state before transitioning to the $^1\Pi_1$ state and later recombining. The slower decay at the interface compared with either of the two bulk media is consistent with the longer time the molecule remains in the excited state, as mentioned above. In addition, as will be shown below, the slower decay at the interface than in bulk water reflects the slower vibrational relaxation of the recombined ICN at the interface. In contrast, the trajectories that ended up as separated I + CN show a diffusive behavior past the 0.6 ps time scale, with the interface result falling in between the results in the bulk phases. The extra separation between the fragments that started on the $^3\Pi_1$ state is due to the extra available translational energy, as will be shown below.

Figure 9 shows that the photodissociation products and the recombined molecules remain largely at the interface region by the end of the 10 ps trajectory. The width of the distribution of the C-atom positions for the trajectories that end up at ICN or INC is about 4.5 Å (full width at half-height), only slightly greater than the 10/90 width of the interface (the distance over which the water density changes from 90% to 10% of the bulk

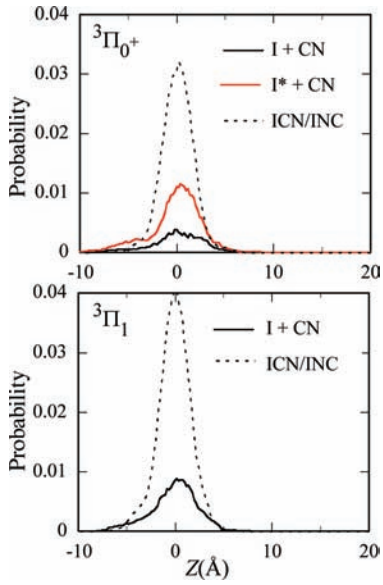

Figure 9. Probability distribution of the C-atom position along the interface normal at $t = 10$ ps following photodissociation of ICN at the water/chloroform interface. Top and bottom panels are for the dissociation starting on the $^3\Pi_{0+}$ and $^3\Pi_1$ excited states, respectively. In each panel, the solid and dotted lines correspond to the C position of the case where the I and CN did not recombine and recombined, respectively, while the red line corresponds to the case where the I ended up at I*. The area under each curve is equal to the total probability of the corresponding channel.

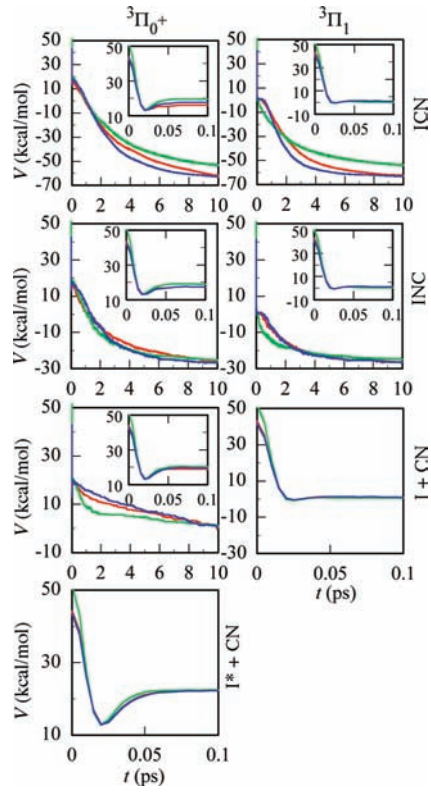

Figure 10. Time-dependent ensemble average of the ICN potential energy following photodissociation of ICN on the $^3\Pi_{0+}$ (left) and $^3\Pi_1$ (right) states. The averages are calculated separately for all the trajectories that end up as ICN, INC, I + CN, and I* + CN, as indicated. In each panel, blue, green, and red lines are for the reaction carried out in bulk water and bulk chloroform and at the water/chloroform interface, respectively. The insert in each panel shows the short time behavior ($t < 0.1$ ps). Note the shorter time scales in the bottom panels on the right and left.

value), which is 4.1 Å. The width of the distribution for the trajectories in which the I and CN did not recombine is much greater, especially for the trajectories where the I is produced on the ground state (due to the larger available translational energy, as will be shown below). Although these fragments did not recombine, they remain for the most part within 5 Å of each side of the Gibbs surface.

Figure 8 shows that by $t = 10$ ps, the average I−CN separation at the interface is 10 Å, while the width of the distribution of the C atoms position along the interface normal (Z direction) is only about 5 Å (solid lines in the two panels of Figure 9). This is consistent with the fact that the cage-escaped fragments correspond to the tail of the Z-position distribution, as well as the fact that many fragments move parallel to the interface (noting that the most likely distribution of the initial ICN direction is parallel to the interface).

3. Energy Disposal. The behavior discussed above can be understood by examining the energy disposal in the different fragments' degrees of freedom.

The average potential energy $\langle V(t)\rangle$ of the ICN gives information about the time scale for the system to relax to the final products. This is shown in Figure 10, in which the ensemble averages are calculated separately depending on the reaction outcome for photodissociation on the $^3\Pi_{0+}$ and the $^3\Pi_1$ states. The insert shows that the outcome of the photodissociation is independent of the initial value of the potential energy. The only difference observed in the various panels is the higher initial value of V for the reaction in bulk $CHCl_3$, discussed previously. The longer time behavior strongly depends on the photodissociation outcome: For the trajectories that end up as ICN, the relaxation to the ground state is fastest in bulk water, slower at the interface, and slowest in bulk $CHCl_3$. By the end of the 10 ps time interval, the system is fully relaxed in bulk water and at the interface but remains vibrationally hot in bulk $CHCl_3$. The variation in the vibrational lifetime in going from bulk water to the interface and to chloroform is consistent with our previous studies on the vibrational relaxation of neutral solutes at the water/CCl_4 interface.[57] The vibrational friction on the ICN vibrational modes at the interface has significant contributions from both water and $CHCl_3$ molecules, giving rise to a value of the vibrational lifetime that is intermediate between that in bulk water (where the friction is the largest) and in bulk $CHCl_3$. Note that the above only applies to the tail of the decay curves. The behavior in the time interval $t < 2$ ps is controlled by the dynamics of the nonadiabatic crossings to the ground state, which, as discussed earlier, is more rapid in bulk $CHCl_3$ than in bulk water, giving rise to the faster decay observed in the potential energy of ICN in bulk $CHCl_3$ on this time scale. This also explains the behavior of $\langle V(t)\rangle$ in INC, since the INC potential well is much shallower than that of ICN, and the net effect is that the relaxation curves leading to ground-state INC look very similar in the three media.

For the trajectories that end up as I + CN starting on the $^3\Pi_1$ state or as I* + CN starting on the $^3\Pi_{0+}$ state, the potential energy reaches the plateau values of 0 and 22 kcal/mol, respectively, by $t = 0.1$ ps, as expected. However, the trajectories that end up as I + CN starting on the $^3\Pi_{0+}$ state must have undergone the $^3\Pi_{0+} \rightarrow {}^1\Pi_1$ transition, which, as discussed above, take place during most of the 10 ps time interval, which is reflected in the behavior depicted in the corresponding panel (second panel from the bottom on the left) of Figure 10. The faster decay in bulk chloroform represents the faster nonadiabatic transitions in this medium, which has been previously discussed.

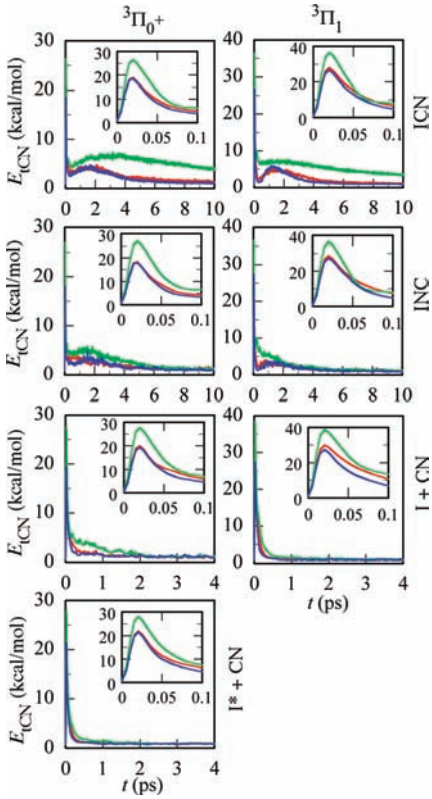

Figure 11. Time-dependent ensemble average of the CN fragment translational energy following photodissociation of ICN on the $^3\Pi_{0+}$ (left) and $^3\Pi_1$ (right) states. The averages are calculated separately for all the trajectories that end up as ICN, INC, I + CN, and I* + CN, as indicated. In each panel, blue, green, and red lines are for the reaction carried out in bulk water and bulk chloroform and at the water/chloroform interface, respectively. The insert in each panel shows the short time behavior ($t < 0.1$ ps). Note the different energy scales of the right and left panels and the shorter time scales for the trajectories that are cage escaped.

Figure 11 shows the time-dependent average of the CN radical translational energy, again calculated separately depending on the reaction outcome for photodissociation on the $^3\Pi_{0+}$ and $^3\Pi_1$ states. The insert shows that the peak energy is achieved in all cases 20 fs after excitation, corresponding to the fragment descent on the potential-energy surface before the solvent molecule had any time to interact with the fragment. As explained earlier, the peak value of the energy is larger in chloroform than in bulk water and at the interface and on the $^3\Pi_1$ compared with the $^3\Pi_{0+}$ state, due to the initial configuration of the FC condition. The subsequent behavior strongly depends on the final photodissociation products, but in all cases the CN translational dynamics in bulk water and at the water/chloroform interface are almost identical but typically quite different from the behavior in bulk chloroform.

For the trajectories that end up as ICN, the rapid decay in the translation energy due to the collision with the solvent shows a rebound as the I and CN recombined to produce vibrationally hot ICN. This relaxes in chloroform much slower than in water or at the water/chloroform interface. The trajectories that end up as INC have much less vibrational excitation, due to the shallower INC well depth. In contrast, the trajectories that end up as I + CN or I* + CN show very rapid translational relaxation that is complete by $t \approx 0.6$ ps, as the multiple collisions with the solvent molecules rapidly transfer the kinetic energy to the solvent bath. This is consistent with the onset of the diffusion motion shown in Figure 8.

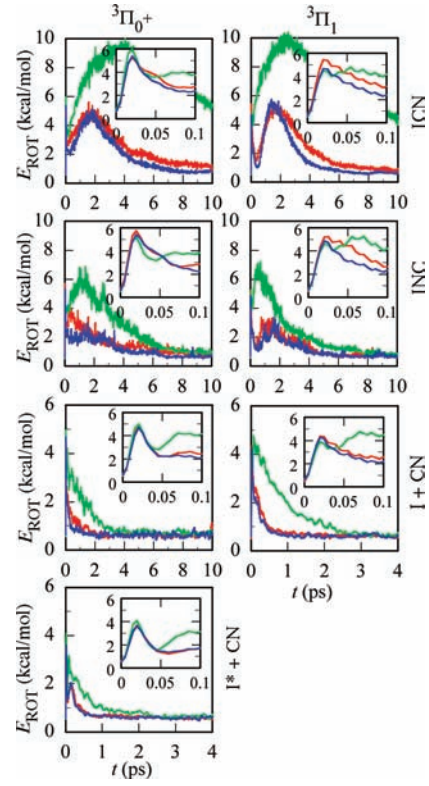

Figure 12. Same as Figure 10 for the CN rotational energy.

The behavior of the iodine-atom translational energy is very similar (not shown), except that the peak energy is about a quarter of the CN translation energy, corresponding approximately to the CN:iodine mass ratio.

We conclude with an examination of the CN radical rotational energy shown in Figure 12. Due to the torque exerted by the excited-state potential-energy surface, the CN radical is produced with substantial rotational excitation, which reaches a value of 5 kcal/mol at $t = 20$ fs, nearly independent of the solvent, the photoproducts, or the initial excited state. However, as is the case with the CN translation energy, trajectories that end up as ICN or INC show substantial bending excitation, which relaxes very fast in bulk water, slightly slower at the interface, and significantly slower in bulk chloroform. In contrast, CN rotation in trajectories that end up as I + CN or I* + CN is very similar in bulk water and at the interface but much slower in chloroform. This is due to the significantly more spherical CN−$CHCl_3$ interaction potential than the CN−H_2O potential and the fact that at the interface the CN must be experiencing contributions from both of these potentials. The rotational excitation of the CN and the subsequent decay can be probed experimentally by following the anisotropy decay of the CN orientation vector.[55,58] The experimental and theoretical study of this phenomenon will be reported elsewhere.[59]

V. Conclusions

The molecular dynamics computer simulations suggest that the photodissociation of ICN at the water/chloroform interface is, in several respects, quite similar to the reaction in bulk water. The energy available to the photodissociation products is similar, reflecting the nearly identical absorption maxima in water and at the interface, both shifted to the blue relative to the location of the absorption spectrum in bulk chloroform. However, the probability for cage escape at the liquid/liquid interface is larger than in the bulk of either liquid. The translational and rotational

relaxation of the CN radical in bulk water is slightly faster than at the water/chloroform interface and typically much faster than the behavior in bulk chloroform. The vibrational relaxation of the ICN and INC products follows a similar relation.

It remains an open question as to whether the current experimental methodology, which is based on picosecond and femtosecond time-resolved probing of the CN radical or the parent molecule and is extensively used to study this reaction in the bulk of these liquids, can be applied to the study of this reaction at the interface. It is also worth extending the theoretical calculations to photodissociation reactions involving reactant and/or product molecules with a significant nonlinear response as a way to improve the ability of experimental detection.

Acknowledgment. This work has been supported by a grant from the National Science Foundation (CHE-0809164). Discussions with Profs. Stephen Bradforth and Richard Stratt and with Chris Rivera about the rotational relaxation of CN and other aspects of ICN photodissociation in liquids are greatly appreciated.

References and Notes

(1) Furlan, A.; Hall, G. E. *J. Chem. Phys.* **1998**, *109*, 10390.
(2) Furlan, A. *J. Phys. Chem. B* **1999**, *103*, 1550.
(3) Graham, J. D.; Roberts, J. T.; Anderson, L. D.; Grassian, V. H. *J. Phys. Chem.* **1996**, *100*, 19551.
(4) Yabushita, A.; Kawasaki, M.; Sato, S. *J. Phys. Chem. A* **2003**, *107*, 1472.
(5) Vieceli, J.; Chorny, I.; Benjamin, I. *J. Chem. Phys.* **2001**, *115*, 4819.
(6) Winter, N.; Benjamin, I. *J. Chem. Phys.* **2004**, *121*, 2253.
(7) Chorny, I.; Vieceli, J.; Benjamin, I. *J. Phys. Chem. B* **2003**, *107*, 229.
(8) Rajesh, C. S.; Thanulingam, T. L.; Das, S. *Tetrahedron* **1997**, *53*, 16817.
(9) Naujok, R. R.; Paul, H. J.; Corn, R. M. *J. Phys. Chem.* **1996**, *100*, 10497.
(10) Naujok, R. R.; Higgins, D. A.; Hanken, D. G.; Corn, R. M. *J. Chem. Soc., Faraday Trans.* **1995**, *91*, 1411.
(11) Higgins, D. A.; Naujok, R. R.; Corn, R. M. *Chem. Phys. Lett.* **1993**, *213*, 485.
(12) Adachi, H.; Sonoki, H.; Hoshino, M.; Wakasa, M.; Hayashi, H.; Miyazaki, Y. *J. Phys. Chem. A* **2001**, *105*, 392.
(13) Solntsev, K. M.; Al-Ainain, S. A.; Il'ichev, Y. V.; Kuzmin, M. G. *J. Phys. Chem. A* **2004**, *108*, 8212.
(14) Tsun-Mei, C.; Dang, L. X.; Peterson, K. A. *J. Phys. Chem. B* **1997**, *101*, 3413.
(15) Lauterbach, M.; Engler, E.; Muzet, N.; Troxler, L.; Wipff, G. *J. Phys. Chem. B* **1998**, *102*, 245.
(16) Hore, D. K.; Walker, D. S.; MacKinnon, L.; Richmond, G. L. *J. Phys. Chem. C* **2007**, *111*, 8832.
(17) Winter, N.; Chorny, I.; Vieceli, J.; Benjamin, I. *J. Chem. Phys.* **2003**, *119*, 2127.
(18) Yabushita, S.; Morokuma, K. *Chem. Phys. Lett.* **1990**, *175*, 518.
(19) Amatatsu, Y.; Yabushita, S.; Morokuma, K. *J. Chem. Phys.* **1994**, *100*, 4894.
(20) Qian, J.; Tannor, D. J.; Amatatsu, Y.; Morokuma, K. *J. Chem. Phys.* **1994**, *101*, 9597.
(21) Fernandez Alberti, S.; Halberstadt, N.; Beswick, J. A.; Echave, J. *J. Chem. Phys.* **1998**, *109*, 2844.
(22) Fernandez Alberti, S.; Echave, J. A.; Engel, V.; Halberstadt, N.; Beswick, J. A. *J. Chem. Phys.* **2000**, *113*, 1027.
(23) Krylov, A. I.; Gerber, R. B. *J. Chem. Phys.* **1997**, *106*, 6574.
(24) Batista, V. S.; Coker, D. F. *J. Chem. Phys.* **1997**, *106*, 7102.
(25) Berendses, H. J. C.; Postma, J. P. M.; Gunsteren, W. F. v.; Hermans, J. In *Intermolecular Forces*; Pullman, B. , Ed.; D. Reidel: Dordrecht,1981; pp 331.
(26) Benjamin, I. Molecular dynamics methods for studying liquid interfacial phenomena. In *Modern Methods for Multidimensional Dynamics Computations in Chemistry*; Thompson, D. L. , Ed.; World Scientific: Singapore, 1998; pp 101.
(27) Kuchitsu, K.; Morino, Y. *Bull. Chem. Soc. Jpn.* **1965**, *38*, 814.
(28) Benjamin, I. *J. Chem. Phys.* **1995**, *103*, 2459.
(29) Hwang, J. K.; King, G.; Creighton, S.; Warshel, A. *J. Am. Chem. Soc.* **1988**, *110*, 5297.
(30) Sprik, M.; Klein, M. L. *J. Chem. Phys.* **1988**, *89*, 7556.
(31) Ahlstrom, P.; Wallqvist, A.; Engstrom, S.; Jonsson, B. *Mol. Phys.* **1989**, *68*, 563.
(32) Wallqvist, A. *Chem. Phys.* **1990**, *148*, 439.
(33) Dang, L. X.; Rice, J. E.; Caldwell, J.; Kollman, P. A. *J. Am. Chem. Soc.* **1991**, *113*, 2481.
(34) Smith, D. E.; Dang, L. X. *J. Chem. Phys.* **1994**, *100*, 3757.
(35) Bader, J. S.; Berne, B. J. *J. Chem. Phys.* **1996**, *104*, 1293.
(36) Morita, A.; Kato, S. *J. Chem. Phys.* **1998**, *109*, 5511.
(37) Small, D. W.; Matyushov, D. V.; Voth, G. A. *J. Am. Chem. Soc.* **2003**, *125*, 7470.
(38) Wallqvist, A. *Chem. Phys. Lett.* **1990**, *165*, 437.
(39) Motakabbir, K.; Berkowitz, M. *Chem. Phys. Lett.* **1991**, *176*, 61.
(40) Chang, T. M.; Dang, L. X. *J. Chem. Phys.* **1996**, *104*, 6772.
(41) Benjamin, I. *Chem. Phys. Lett.* **1998**, *287*, 480.
(42) Dang, L. X.; Chang, T. *J. Phys. Chem. B* **2002**, *106*, 235.
(43) Jungwirth, P.; Tobias, D. J. *J. Phys. Chem. A* **2002**, *106*, 379.
(44) Li, Z. M.; Fang, J. Y.; Martens, C. C. *J. Chem. Phys.* **1996**, *104*, 6919.
(45) Tully, J. C. Nonadiabatic Dynamics. In *Modern Methods for Multidimensional Dynamics Computations in Chemistry*; Thompson, D. L., Ed.; World Scientific: Singapore, 1998; p 34.
(46) Tully, J. C. *J. Chem. Phys.* **1990**, *93*, 1061.
(47) Press, W. H.; Teukolsky, S. T.; Vetterling, W. T.; Flannery, B. P. *Numerical Recipes in C*, 2nd ed.; Cambridge University Press: Cambridge, U.K., 1992.
(48) Warshel, A.; Weiss, R. M. *J. Am. Chem. Soc.* **1980**, *102*, 6218.
(49) Villa, J.; Bentzien, J.; Gonzalez-Lafont, A.; Lluch, J. M.; Bertran, J.; Warshel, A. *J. Comput. Chem.* **2000**, *21*, 607.
(50) Margulis, C. J.; Coker, D. F. *J. Chem. Phys.* **2000**, *113*, 6113.
(51) Day, T. J. F.; Soudackov, A. V.; Cuma, M.; Schmitt, U. W.; Voth, G. A. *J. Chem. Phys.* **2002**, *117*, 5839.
(52) Raftery, D.; Gooding, E.; Romanovsky, A.; Hochstrasser, R. M. *J. Chem. Phys.* **1994**, *101*, 8572.
(53) Wan, C.; Gupta, M.; Zewail, A. H. *Chem. Phys. Lett.* **1996**, *256*, 279.
(54) Larsen, J.; Madsen, D.; Poulsen, J. A.; Poulsen, T. D.; Keiding, S. R.; Thogersen, J. *J. Chem. Phys.* **2002**, *116*, 7997.
(55) Moskun, A. C.; Bradforth, S. E. *J. Chem. Phys.* **2003**, *119*, 4500.
(56) Landau, L. D.; Lifshitz, E. M. *Quantum Mecahnics: Non-relativistic Theory*; Pergamon: New York, 1977.
(57) Benjamin, I. *J. Chem. Phys.* **2004**, *121*, 10223.
(58) Moskun, A. C.; Jailaubekov, A. E.; Bradforth, S. E.; Tao, G.; Stratt, R. M. *Science* **2006**, *311*, 1907.
(59) Rivera, C.; Bradforth, S. E.; Benjamin, I. Manuscript in preparation.

JP900153J